Iron and Molybdenum Extended X-ray Absorption Fine Structure Studies of Double-Cubane Clusters Containing $MoFe_3S_4$ Cores

Mark R. Antonio,[1a,b] Boon-Keng Teo,*[1c] Walter E. Cleland,[1a] and Bruce A. Averill*[1a,d]

Contribution from the Department of Chemistry, Michigan State University, East Lansing, Michigan 48824, and Bell Laboratories, Murray Hill, New Jersey 07974.
Received September 20, 1982

Abstract: The Mo and Fe K-edge extended X-ray absorption fine structure (EXAFS) of $(Bu_4N)_3[Mo_2Fe_6S_8(SEt)_9]$ (**1**) $(Et_4N)_3[Mo_2Fe_6S_9(SEt)_8]$ (**2**), and $(Et_3NCH_2Ph)_3[Mo_2Fe_6S_8(SEt)_3(OPh)_6]$ (**3**) have been measured (in transmission mode) and analyzed. These clusters are known (**1** and **2**) or believed (**3**) to have the so-called double-cubane structures with two $MoFe_3S_4$ cubes. The interatomic distances, determined by curve fitting with theoretical phase and amplitude functions, agree well with crystallographic results. Using **1** (whose structure is most accurately known) as the model, the number of atoms neighboring the Mo and the Fe atoms can be determined to a satisfactory degree for the crystallographically disordered **2** and the structurally yet unknown **3**. Curve fitting of the Mo EXAFS with a two-term expression yields average Mo–S (sulfide) and Mo–Fe distances and coordination numbers, whereas curve fitting with a three-term expression yields average Mo–S (sulfide), Mo–S′ (thiolate), and Mo–Fe distances and coordination numbers. The original Mo EXAFS spectrum of **2** reported in the literature has been shown to be due to an approximately equimolar mixture of **1** and **2**. The Fourier transforms of the Fe EXAFS of **1** and **2** exhibit only one peak, due to Fe–S backscattering, whereas the corresponding transform of **3** shows only two peaks, due to Fe–O and Fe–S backscatterings. The unexpected finding of the absence of backscattering due to neighboring Fe and Mo atoms is explained in terms of cancellation of the Fe–Fe and Fe–Mo waves, since the total phase difference, $\phi_{Mo}{}^b - \phi_{Fe}{}^b$, is approximately π radians for $k \gtrsim 7$ Å^{-1} (according to theory). In a novel extension of the EXAFS beat node method, modified EXAFS amplitude envelope and phase functions were determined to illustrate the Fe–Fe and Fe–Mo distance dependence of the cancellation of the back-scattered waves. A difference technique was used to determine, in a stepwise manner, the metal–ligand and the metal–metal distances and coordination numbers. The apparent lack of a metal–metal peak in the Fourier transforms of the Fe EXAFS of **1**–**3** makes these clusters inadequate as models for the Fe EXAFS of the FeMo cofactor.

An extensive series of synthetic molybdenum–iron–sulfur clusters with the $MoFe_3S_4$ cubane core is known.[2,3] The molecular structures of some ten Mo–Fe–S double-cubane[4,5a–f] and two single-cubane[5g,h] clusters have been determined by X-ray diffraction methods. Such clusters are of special importance, in that they have several features that are similar to those of the molybdenum sites in the MoFe protein[6,7] and the FeMo cofactor[6b,7] of the enzyme nitrogenase. The Mo K-edge extended X-ray absorption fine structure (EXAFS) data reported for $[Mo_2Fe_6S_9(SEt)_8]$,[3–5a,b] $[Mo_2Fe_6S_8(SEt)_9]$,[3–5b] and the MoFe protein[6] and FeMo cofactor[7] of nitrogenase indicate that the local environment about Mo in each may be similar, at least in terms of the identity, number, and distances of nearest neighbors. The double-cubane compounds thus serve as models for the Mo EXAFS of nitrogenase. We have, however, found that these clusters do not serve as adequate models for the Fe EXAFS of the FeMo cofactor of nitrogenase, because of the distinctive differences in their Fe EXAFS spectra. We report here the Mo K-edge EXAFS of $(Bu_4N)_3[Mo_2Fe_6S_8(SEt)_9]$ (**1**), $(Et_4N)_3[Mo_2Fe_6S_9(SEt)_8]$ (**2**), and the new cluster $(Et_3NCH_2Ph)_3[Mo_2Fe_6S_8(SEt)_3(OPh)_6]$ (**3**), known (**1** and **2**) or proposed (**3**) to have the double-cubane structure. The Mo EXAFS data first reported[5a] for **2** were found to be those of a mixture of **1** and **2**. The Fe K-edge EXAFS of **1**–**3** are also reported here for the first time, with some rather surprising results. Comparison with the recently reported Fe EXAFS of the FeMo cofactor[8] indicates that compounds **1**–**3** are not appropriate models for the iron sites in the FeMo cofactor.

Experimental Section

Compounds **1** and **2** were prepared according to literature methods[5b] and were checked for purity by ^{1}H NMR spectroscopy. After multiple recrystallizations of **2**, the final product contained less than 1% of the $[Mo_2Fe_6S_8(SEt)_9]^{3-}$ salt. The novel cluster **3**, with oxygen ligation to iron, was obtained by ligand substitution of the terminal ethanethiolates in **1** by phenol.[9] All available chemical and spectroscopic evidence are consistent with a double-cubane structure for **3**.

The X-ray absorption data were collected[10] at CHESS and SSRL.

(1) (a) Michigan State University. (b) Union Carbide Summer Research Fellow, 1982. Current address: The Standard Oil Company (Ohio), Warrensville Research Center, Cleveland, OH 44128. (c) Bell Laboratories. (d) Current address: Department of Chemistry, University of Virginia, Charlottesville, Virginia 22901.

(2) Holm, R. H. *Chem. Soc. Rev.* **1981**, *10*, 455.

(3) Averill, B. A. *Struct. Bonding (Berlin)* **1983**, *53*, 59.

(4) (a) Christou, G.; Garner, C. D.; Mabbs, F. E.; King, T. J. *J. Chem. Soc., Chem. Commun.* **1978**, 740. (b) Christou, G.; Garner, C. D.; Mabbs, F. E.; Drew, M. G. B. *Ibid.* **1979**, 91. (c) Acott, S. R.; Christou, G.; Garner, C. D.; King, T. J.; Mabbs, F. E.; Miller, R. M. *Inorg. Chim. Acta* **1979**, *35*, L337. (d) Garner C. D.; Acott, S. R.; Christou, G.; Collison, D.; Mabbs, F. E.; Miller, R. M. In "Current Perspectives in Nitrogen Fixation"; Gibson, A. H., Newton, W. E., Eds.; Australian Academy of Science: Canberra, Australia, 1981; pp 40–43.

(5) (a) Wolff, T. E.; Berg J. M.; Warrick, C.; Hodgson, K. O.; Holm, R. H.; Frankel, R. B. *J. Am. Chem. Soc.* **1978**, *100*, 4630. (b) Wolff, T. E.; Berg, J. M.; Hodgson, K. O.; Frankel, R. B.; Holm, R. H. *Ibid.* **1979**, *101*, 4140. (c) Wolff, T. E.; Berg, J. M.; Power P. P.; Hodgson, K. O.; Holm, R. H.; Frankel, R. B. *Ibid.* **1979**, *101*, 5454. (d) Wolff, T. E.; Berg, J. M.; Power, P. P.; Hodgson, K. O.; Holm, R. H. *Inorg. Chem.* **1980**, *19*, 430. (e) Armstrong, W. H.; Holm, R. H. *J. Am. Chem. Soc.* **1981**, *103*, 6246. (f) Christou, G.; Mascharak, P. K.; Armstrong, W. H.; Papaefthymiou, G. C.; Frankel, R. B.; Holm, R. H. *Ibid.* **1982**, *104*, 2820. (g) Wolff, T. E.; Berg, J. M.; Holm, R. H. *Inorg. Chem.* **1981**, *20*, 174. (h) Armstrong, W. H.; Mascharak, P. K.; Holm, R. H. *Ibid.* **1982**, *21*, 1699.

(6) (a) Cramer, S. P.; Hodgson, K. O.; Gillum, W. O.; Mortenson, L. E. *J. Am. Chem. Soc.* **1978**, *100*, 3398. (b) Cramer, S. P.; Gillum, W. O.; Hodgson, K. O.; Mortenson, L. E.; Stiefel, E. I.; Chisnell, J. R.; Brill, W. J.; Shah, V. K. *Ibid.* **1978**, *100*, 3814.

(7) (a) Newton, W. E.; McDonald, J. W.; Friesen, G. D.; Burgess, B. K.; Conradson, S. D.; Hodgson, K. O. In "Current Perspectives in Nitrogen Fixation"; Gibson, A. H., and Newton, W. E., Eds.; Australian Academy of Science: Canberra, Australia, 1981; pp 30–39. (b) Burgess, B. K.; Yang, S. S.; You, C. B.; Li, J. G.; Friesen, G. D.; Pan, W. H.; Stiefel, E. I.; Newton, W. E.; Conradson, S. D.; Hodgson, K. O. *Ibid.*, pp 71–74.

(8) Antonio, M. R.; Teo, B.-K.; Orme-Johnson, W. H.; Nelson, M. J.; Groh, S. E.; Lindahl P. A.; Kauzlarich, S. M.; Averill, B. A. *J. Am. Chem. Soc.* **1982**, *104*, 4703.

(9) Cleland, W. E.; Averill, B. A., manuscript in preparation.

0002-7863/83/1505-3477$01.50/0

Tables of the raw Fe and Mo K-edge X-ray absorption data, in the form $\ln I_0/I$ vs. E (in eV), for **1-3** are presented in the supplementary material. The data reduction[11] and curve fitting were performed as detailed elsewhere.[12,13] The background-subtracted Mo and Fe EXAFS spectra, $k^3\chi(k)$ vs. k (in Å^{-1}), of **1-3** are shown in Figures A-G (supplementary material).

Results and Discussion

Mo K-Edge Data. Fourier transforms of the normalized Mo EXAFS, $k^3\chi(k)$ vs. k, of **1-3** exhibit two principal peaks, which are assigned to Mo-S and Mo-Fe back-scatterings (in increasing order of distance), cf. Figure 1a-c for **1-3**, respectively. The Fourier transform of **3** (Figure 1c) is virtually identical with that of **1**, suggesting that the Mo environment of **3** is similar to that of **1**. The magnitude of the Mo-S Fourier transform peaks, which presumably are due to inorganic sulfide (S) and/or mercaptide (S′) back-scatterings, qualitatively indicate a larger number of sulfur neighbors in the first coordination sphere of molybdenum in **2** than in either **1** or **3** (i.e., the Mo-S peak in **2** is larger than those in **1** and **3**). Also, the shapes of the Mo-S peaks are considerably different, suggesting a substantially different radially averaged sulfur environment about molybdenum in each cluster. For example, the peak centered at 1.90 Å due to sulfur back-scattering in **1** is narrow (fwhm 0.29 Å) and symmetrical (neglecting the side lobe at 1.62 Å, due to Fourier truncation error), whereas the Mo-S peak at 1.87 Å in the spectrum of **2** is significantly broader (fwhm 0.54 Å) and unsymmetrical. These features are diagnostic of the structural differences between the MoS_3Mo units in double-cubane clusters containing the Mo-$(\mu_2\text{-SEt})_3$Mo and the Mo$(\mu_2\text{-SEt})_2(\mu_2\text{-S})$Mo units (cf. Figure 1a,b for **1** and **2**, respectively). A unique characterization of the MoS_3Mo unit in **2** was not possible by X-ray diffraction methods, owing to crystallographic disorder.[5b] By curve fitting the EXAFS data of **1-3** (vide infra), we have quantitatively examined the structural features of the sulfur coordination spheres about molybdenum, regardless of static disorder.

The first report of the Mo EXAFS spectrum (weighted by k^2) of the purported cluster $(Et_4N)_3[Mo_2Fe_6S_9(SEt)_8]$ (**2**) was given by Wolff et al.[5a] These data were reweighted by k^3 and the Fourier transform was presented by Teo and Averill.[14] We note that the Fourier transform of the original Mo EXAFS[5a] of **2** is distinctly different from Figure 1b reported here. In fact, the original data[5a] look like the arithmetic average of those of **1** (Figure 1a) and **2** (Figure 1b) which is shown in Figure 1d. (For the corresponding k space data of Figures 1a, 1b, and 1d, see Figures A, B, and D in the supplementary material.) This observation, in conjunction with our curve-fitting analysis (vide infra), leads us to believe that the Mo EXAFS data originally reported[5a] for **2** are, very likely, those of an approximately equimolar mixture of **1** and **2**.

The contributions of the two peaks in the Fourier transforms of **1-3** were isolated from the distance (Å) space with smooth window functions (dashed curves, Figures 1a-c, for **1-3**, respectively) and back-transformed to k (Å^{-1}) space. The resulting Fourier filtered $k^3\chi(k)$ vs. k data, truncated at 3 and 14.5 Å^{-1} and shown in Figure 2a-c (solid curves) for **1-3**, were employed in the nonlinear least-squares curve fitting[15] with the conventional formulation of the EXAFS phenomenon based on short-range single-scattering theory:[16-19]

$$k^3\chi(k) = \sum_j B_j F_j(k_j) k_j^2 \exp(-2\sigma_j^2 k_j^2) \sin [2k_j r_j + \phi_j(k_j)] / r_j^2 \quad (1)$$

Theoretical amplitude $F_j(k_j)$ and phase $\phi_j(k_j)$ functions calculated by Teo and Lee[12a] were used in the curve fittings. For each k value, $F(k)$ and $\phi(k)$ were interpolated from the theoretical values.[20] Here σ_j is the Debye-Waller factor and the scale factor is $B_j = S_j N_j$, where S_j is the amplitude reduction factor and N_j is the number of atoms of the jth type at a distance r_j away from the X-ray-absorbing atom.

The filtered spectra of the Mo EXAFS of **1-3** were fit with both a two-term model[21a] (eq 1 where j = S, Fe) and a three-term model[21b] (j = S, S′, Fe). Figure 2a-c shows the best fit (dashed curves) of the two-term EXAFS model to the Fourier filtered data (solid curves) of **1-3**. It can be seen from Figure 2a-c that the two-term fits to the Mo EXAFS of **1-3** are satisfactory, as judged by the goodness of the fits[15b] (Σ^2 = 10, 28, and 17, respectively). The goodness of the three-term fits[15b] improves by ca. 1.5-2.5 (Σ^2 = 4, 16-19, and 7 for **1-3**), compared with the two-term fits. With

(10) The measurements were performed at the Cornell High Energy Synchrotron Source (C-2 beam line: energy resolution, ca. 5 eV at 20 KeV and ca. 1 eV at 7 KeV), operating at 5.18 GeV with 4-12 mA of stored current, and at the Stanford Synchrotron Radiation Laboratory (beam line I-5: energy resolution at 20 KeV ca. 5 eV) operating at 3.0 GeV with 50-80 mA of stored current. The Fe data of **1-3** and the Mo data of **1** and **2** were recorded at CHESS. Only the Mo data of **3** were recorded at SSRL. The polycrystalline samples were run as boron nitride pellets. All operations were carried out under nitrogen. The incident beam was monochromated with Si(220) crystals at both CHESS and SSRL. The harmonic content of the beam was significantly reduced by detuning the monochromator prior to each scan. The incident (I_0) and transmitted (I) beam intensities were monitored by ionization chambers (flow type); argon was used in both chambers for the Mo edge and a combination of nitrogen (I_0) and argon (I) was used for the Fe edge. The absorption data were recorded at ambient temperature with an integration time of ca. 1-2 s/point over an energy range of ca. 19800-20900 eV for Mo and ca. 7010-7920 eV for Fe, containing either 150 or 205 points (in steps of constant k) for CHESS data and 450 points (in steps of constant E) for SSRL data.

(11) The experimental energy thresholds (E_0) were chosen at 19980 eV for the Mo data of **1** and **2** and 19858 eV for **3** and at 7130 eV for all Fe data. The edge position energies (E_0^p) were determined to be 19983, 19981, and 19861 eV for the Mo data and 7114, 7114, and 7119 eV for the Fe data of **1**, **2**, and **3**, respectively. The data were weighted by k^3, and the background was removed by using five sets (ca. 3.0 Å^{-1} each) of cubic spline functions. The EXAFS was normalized by dividing by the edge jumps and also corrected for the falloff in the absorption cross section according to Victoreen's equation.

(12) (a) Teo, B.-K.; Lee, P. A. *J. Am. Chem. Soc.* **1979**, *101*, 2815. (b) Teo, B.-K.; Shulman R. G.; Brown, G. S.; Meixner A. E. *Ibid.* **1979**, *101*, 5624. (c) Teo, B.-K. *Acc. Chem. Res.* **1980**, *13*, 412. (d) Teo, B.-K. in "EXAFS Spectroscopy: Techniques and Applications"; Teo, B.-K., Joy, D. C., Eds.; Plenum Press: New York, 1981; pp 15-38. (e) Teo, B.-K.; Antonio, M. R.; Averill, B. A. *J. Am. Chem. Soc.* in press.

(13) Lee, P. A.; Citrin, P. H.; Eisenberger, P.; Kincaid, B. M. *Rev. Mod. Phys.* **1981**, *53*, 769.

(14) Teo, B.-K.; Averill, B. A. *Biochem. Biophys. Res. Commun.* **1979**, *88*, 1454 (cf. Figure 2b in this reference).

(15) (a) A Bell Labs fitting program that incorporates Marquardt's scheme for iterative estimation of nonlinear least-squares parameters via a compromise combination of gradient (when far from convergence) and Taylor series (when close to convergence) methods; see: Marquardt, D. W. *J. Soc. Ind. Appl. Math.* **1963**, *11*, 431. (b) The nonlinear least-squares refinements were based upon the minimization of the sum of squares of the residuals, $\Sigma^2 = \sum_i [k^3\chi(k)_i - k^3\chi'(k)_i]^2$. $k^3\chi(k)$ and $k^3\chi'(k)$ are the calculated and the observed EXAFS, respectively, and i runs through all the data points.

(16) (a) Sayers, D. E.; Lytle, F. W.; Stern, E. A. in "Advances in X-ray Analysis"; Henke, B. L., Newkirk, J. B., Mallett, R. G., Eds.; Plenum Press: New York, 1970; Vol. 13, pp 248-271. (b) Stern, E. A. *Phys. Rev. B* **1974**, *10*, 3027. (c) Sayers, D. E.; Stern, E. A.; Lytle, F. W. *Phys. Rev. Lett.* **1971**, *27*, 1204. (d) Lytle, F. W.; Sayers, D. E.; Stern, E. A. *Phys. Rev. B* **1975**, *11*, 4825. (e) Stern, E. A.; Sayers, D. E.; Lytle, F. W. *Phys. Rev. B* **1971**, *11*, 4836.

(17) Ashley, C. A.; Doniach, S. *Phys. Rev. B* **1975**, *11*, 1279.

(18) (a) Lee, P. A.; Pendry, J. B. *Phys. Rev. B* **1975**, *11*, 2795. (b) Lee, P. A.; Beni, G. *Phys. Rev. B* **1977**, *15*, 2862.

(19) Kincaid, B. M.; Eisenberger, P. *Phys. Rev. Lett.* **1975**, *34*, 1361.

(20) The theoretical values of the EXAFS functions, calculated at discrete intervals in k (Å^{-1}) space, were obtained in ref 12a: from Table VII for the central atom phase $\phi_{Mo}{}^a$ and $\phi_{Fe}{}^a$ (calculated by using Herman-Skillman wave functions); from Table II for the back-scattering phases $\phi_S{}^b$ and $\phi_{Fe}{}^b$ (calculated by using Clementi-Roetti wave functions); from Table V for the back-scattering phase $\phi_{Mo}{}^b$ (calculated by using Herman-Skillman wave functions); from Table I for the back-scattering amplitudes F_S and F_{Fe} (calculated by using Clementi-Roetti wave functions); from Table IV for the back-scattering amplitude F_{Mo} (calculated by using Herman-Skillman wave functions). Oxygen phase $\phi_O{}^b$ and amplitude F_O functions (calculated by using Herman-Skillman wave functions) were obtained from the following: Teo, B.-K. *J. Am. Chem. Soc.* **1981**, *103*, 3990 (Table II supplementary material, for β = 180°).

(21) (a) Eight parameters were varied in the nonlinear least-squares curve fitting: two scale factors, B_S and B_{Fe}; two Debye-Waller factors, σ_S and σ_{Fe}; two distances, r_S and r_{Fe}; and two threshold energy differences, ΔE_{0S} and ΔE_{0Fe}. (b) Eleven parameters were varied in the nonlinear least-squares curve fitting; B_S, $B_{S'}$, and B_{Fe}; σ_S and σ_{Fe} (the single Debye-Waller term σ_S, common to both the sulfide and mercaptide back-scattering terms, was refined herein); r_S, $r_{S'}$, and r_{Fe}; and ΔE_{0S}, $\Delta E_{0S'}$ and ΔE_{0Fe}. (c) Six parameters were varied in the nonlinear least-squares curve fitting: B_{Fe} and B_{Mo}; r_{Fe} and r_{Mo}; and ΔE_{0Fe} and ΔE_{0Mo}. Both σ_{Fe} and σ_{Mo} were fixed at 0.075 Å in the refinements in order to avoid singularities and unrealistic fitting minima.

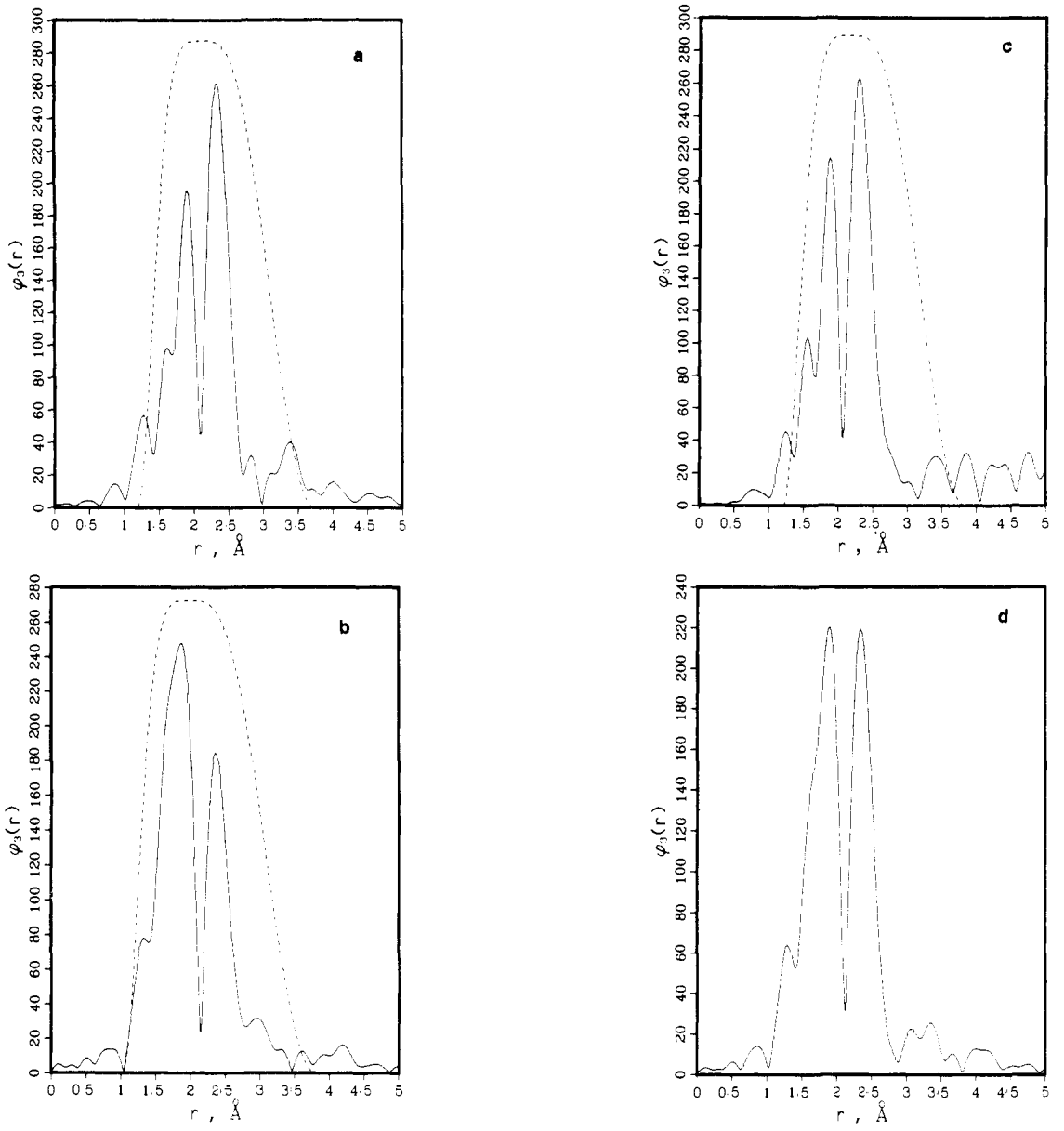

Figure 1. Fourier transforms (solid curves) $\phi_3(r)$ vs. r (Å; before phase shift correction), of the background-subtracted $k^3\chi(k)$ vs. k molybdenum EXAFS spectra, along with the filtering windows (dashed curves), for (a) $(Bu_4N)_3[Mo_2Fe_6S_8(SEt)_9]$; (b) $(Et_4N)_3[Mo_2Fe_6S_9(SEt)_8]$; (c) $(Et_3NCH_2Ph)_3[Mo_2Fe_6S_8(SEt)_3(OPh)_6]$; and (d) a calculated average spectrum of the two preceding clusters in a and b.

both the two- and three-term curve fitting models, the interatomic distances obtained from the best fits, based on theoretical functions (BFBT), agree to within ca. 1% of the available single-crystal X-ray crystallographic results (Table Ia). The coordination numbers presented in Table I were calculated at the best fit Debye–Waller factors, according to a method similar to that described elsewhere,[12e] with **1** as the model compound for the Mo–S, Mo–S′, and Mo–Fe interactions in **2** and **3**. The results (cf. Table Ia) are in good agreement with crystallographical findings. It is interesting to note that the coordination numbers obtained from our analysis of the previously published[5a] data for **2**, with the two-term model (vide supra), correspond almost exactly to the arithmetic mean of the results obtained from the pristine samples, **1** and **2** (this work, Table Ia). In a recent report[7a] on the Mo EXAFS of nitrogenase and several Mo–Fe–S clusters, the Fourier transform of the Mo EXAFS of **2** was presented. These data, although not analyzed in detail, appear to be entirely consistent with the data reported herein for **2**.

The regression coefficients for the ΔE_0 vs. Δr and the B vs. σ correlation curves for the two-term and three-term fits of the Mo EXAFS are tabulated in Table II (cf. supplementary material) and the FABM[12e] results (fine adjustment based on model) are listed in Table III (cf. supplementary material). Since the FABM results are not significantly different from the BFBT results listed in Table Ia (with the exception of Mo–S distances of **2** for the three-term fits, where FABM values of 2.360, 2.357, and 2.355 Å for fits i–iii, respectively), they will not be discussed here.

Fe K-edge Data. Fourier transforms of the Fe EXAFS of **1** and **2** exhibit only *one* peak, due to Fe–S back-scattering, whereas the Fourier transform of the Fe EXAFS of **3** shows only *two* peaks, due to Fe–O and Fe–S back-scatterings (Figure 3a–c). The apparent lack of Fe–Fe and/or Fe–Mo backscatterings in these Fourier transforms is unexpected, since the $MoFe_3S_4$ cores of **1–3** are structurally similar to the Fe_4S_4 cubane cores of the well-characterized $[Fe_4S_4(SR)_4]^{2-}$[22,23] complexes, which exhibit distinct second-shell Fe–Fe peaks in their Fourier transforms.[6a,12b]

The absence of back-scattering due to neighboring Fe and Mo atoms in the Fe EXAFS of **1–3** is due to a combination of several effects: (i) the total phase difference, $\phi_{Mo}{}^b - \phi_{Fe}{}^b$, which is approximately π radians for $k \gtrsim 7$ Å^{-1} (according to the theoretical

(22) Averill, B. A.; Orme-Johnson, W. H. In "Metal Ions in Biological Systems"; Sigel, H., Ed.; Marcel Dekker: New York, 1978; Vol. VII, pp 127–183.
(23) Holm, R. H.; Ibers, J. A. In "Iron–Sulfur Proteins"; Lovenberg, W., Ed.; Academic Press: New York, 1977; Vol. III, pp 205–281.

Table I. Best Fit (Based on Theoretical Functions) Least-Squares Refined Interatomic Distances (r, Å), Energy Threshold Differences (ΔE_0^P, eV), Debye-Waller Factors (σ, Å), scale factors (B), and Coordination Number (N)[a] with Standard Deviations in Parentheses

(a) Mo K-Edge EXAFS of $(n\text{-}Bu_4N)_3[Mo_2Fe_6S_8(SEt)_9]$ (1), $(Et_4N)_3[Mo_2Fe_6S_9(SEt)_8]$ (2), and $(Et_3NCH_2Ph)_3[Mo_2Fe_6S_8(SEt)_3(OPh)_6]$ (3)

term		1[b]	2[b]	2[c]	3
		Two-Term Fit			
Mo-S	r	2.342 (12)	2.337 (19)	2.323 (14)	2.338 (14)
	ΔE_0^{Pd}	−1.62	−2.73	−4.77[e]	−3.00
	σ	0.025 (22)	0.066 (15)	0.035 (25)	0.000 (39)
	B	0.760	2.028	1.067	0.721
	N	3.0 (5)	4.9 (11)	3.8 (8)	3.2 (10)
Mo-Fe	r	2.729 (12)	2.762 (24)	2.738 (14)	2.734 (17)
	ΔE_0^{Pd}	−5.97	0.22	−2.60[e]	−8.74
	σ	0.051 (12)	0.051 (28)	0.046 (17)	0.065 (13)
	B	1.136	0.831	0.904	1.538
	N	3.0 (6)	2.2 (10)	2.6 (7)	3.1 (8)

term		1[b]	2 i[f]	2 ii[f]	2 iii[f]	3
			Three-Term Fit			
Mo-S	r	2.358 (9)	2.303 (37)	2.281 (47)	2.292 (28)	2.360 (12)
	ΔE_0^{Pd}	2.23	−7.87	−10.96	−15.76	2.48
	σ	0.034 (9)	0.050 (37)	0.039 (35)	0.060 (19)	0.026 (19)
	B	0.949	1.208	0.859	1.288	0.996
	N	3.0 (4)	3.0 (22)	2.5 (23)	2.8 (9)	3.5 (6)
Mo-S′	r	2.584 (16)	2.425 (36)	2.402 (42)	2.613 (28)	2.564 (18)
	ΔE_0^{Pd}	10.08	9.09	6.00	−28.06	7.67
	σ	0.034 (9)	0.050 (37)	0.039 (35)	0.060 (19)	0.026 (19)
	B	0.680	0.664	0.865	1.329	0.881
	N	3.0 (4)	2.2 (10)	3.5 (11)	3.9 (13)	3.1 (7)
Mo-Fe	r	2.762 (17)	2.756 (23)	2.751 (23)	2.734 (22)	2.791 (22)
	ΔE_0^{Pd}	3.22	−1.58	−2.53	−6.35	2.21
	σ	0.058 (10)	0.043 (30)	0.050 (22)	0.051 (17)	0.043 (31)
	B	0.919	0.765	0.863	1.051	0.725
	N	3.0 (5)	3.3 (12)	3.3 (12)	4.0 (11)	3.2 (13)

(b) Fe K-edge EXAFS of 1-3

term		1	2	3
Fe-O	r			1.872 (29)
	ΔE_0^{Pd}			17.94
	σ			0.000 (48)
	B			0.319
	N			1.4 (5)[g]
Fe-S	r	2.253 (17)	2.255 (16)	2.261 (22)
	ΔE_0^{Pd}	6.62	7.44	5.52
	σ	0.055 (17)	0.060 (14)	0.070 (17)
	B	1.445	1.290	1.618
	N	4.0 (9)	3.3 (7)	3.6 (10)
Fe-Fe	r	2.661 (14)	2.697 (14)	
	ΔE_0^{Pd}	9.37	15.88	
	σ	0.075[h]	0.075[h]	
	B	0.257	0.215	
	N	2.0 (4)	1.7 (2)	
Fe-Mo	r	2.714 (17)	2.732 (11)	
	ΔE_0^{Pd}	9.83	10.38	
	σ	0.075[h]	0.075[h]	
	B	0.146	0.081	
	N	1.0 (3)	0.6 (2)	

[a] Since the Debye-Waller factors are dissimilar for these compounds, the coordination numbers $N_{2,3}$ for compound 2 and 3 were calculated by using the amplitude reduction factor $S_{2,3}^*$ obtained from the B vs. σ correlation curves of compound 1 (cf. Table II, supplementary material) at the best fit $\sigma_{2,3}$ values (listed here) of compounds 2 and 3. That is, $S^* = B_1/N_1$ (at $\sigma_{2,3}$), then $N_{2,3} = B_{2,3}/S^*$ (at $\sigma_{2,3}$) for each term. Here the subscripts refer to compound numbers. [b] This work. The average crystallographically determined distances[5b] in $(Et_3NCH_2Ph)_3[Mo_2Fe_6S_8(SEt)_9]$ are as follows: Mo-S, 2.351 (3) Å; Mo-S′, 2.567 (4) Å; Mo-Fe, 2.723 (2) Å. The average crystallographic distances[5b] for 2 are as follows: Mo-S, 2.340 (3) Å; Mo-Fe, 2.730 (2) Å. The Mo-S′ distance is not uniquely defined owing to crystallographic disorder.[5b] [c] These results were obtained from our analysis (with k^3 weighting) of the first published Mo EXAFS spectrum[5a] of the purported 2. [d] These standardized energy threshold differences ΔE_0^P were obtained according to $\Delta E_0^P = \Delta E_0 + E_0^{exp} - E_0^P$.[12e] Here ΔE_0 was the least-squares refined energy threshold difference, E_0^{exp} was the experimentally chosen energy threshold,[11] and E_0^P was the edge position energy defined as the photon energy at half-height of the edge jump. [e] These values were obtained by assuming $E_0^{exp} = E_0^P$ (both of which are unavailable) in the equation for footnote d, above and therefore may not be correct. [f] The relative goodness of fits are 18.9, 17.8, and 16.3 for the three statistically equivalent fits i-iii, respectively. [g] Number of oxygen neighbors based upon the iron transmission EXAFS analysis[26a] of the model compound $(Et_4N)_2[Fe_4S_4(OPh)_4]$.[26b,c] [h] These Debye-Waller factors were fixed in the refinements.[21c] The refined values for σ_{Fe} and σ_{Mo}, obtained by curve fitting with eq 1, are 0.062 (10) and 0.123 (15) Å for 1, respectively, and 0.016 (32) and 0.023 (18) Å for 2, respectively.

functions,[12a] Figure 4a); (ii) the distance difference, $\Delta r = r_{Fe-Mo} - r_{Fe-Fe}$, between the two Fe and one Mo scatterers; (iii) the back-scattering amplitude characteristics, F_{Mo} and F_{Fe} (Figure 4b); (iv) differences between the Debye–Waller terms, σ_{Mo} and σ_{Fe}; (v) the ratio of number of neighbors N_{Fe}:N_{Mo}. Of these five factors, the phase and amplitude differences, as well as similar Debye–Waller terms, are common to the Fe EXAFS of all single- or double-cubane type clusters containing the $MoFe_3S_4$ core, and

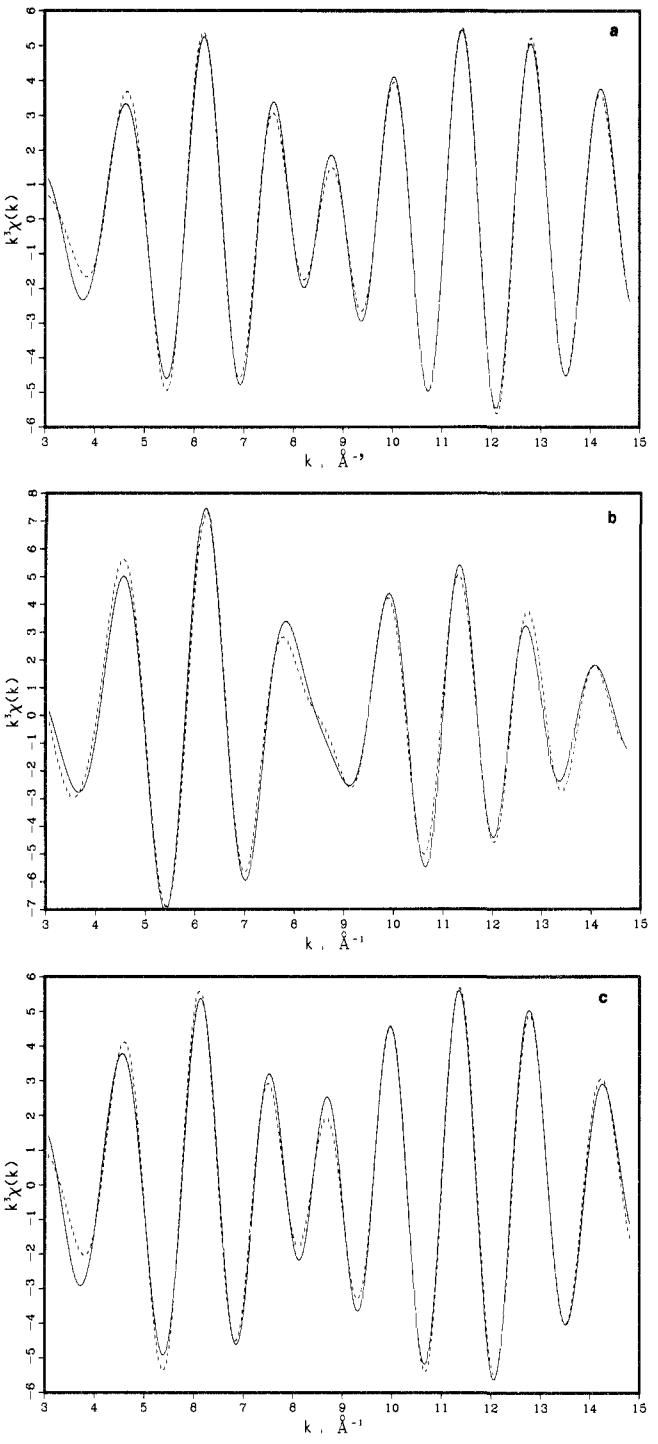

Figure 2. The Fourier filtered $k^3\chi(k)$ vs. k molybdenum EXAFS spectra (solid curves) and the two-term (Mo–S, Mo–Fe) nonlinear least-squares best fits (dashed curves), based on theoretical functions, to the filtered EXAFS of (a) $(Bu_4N)_3[Mo_2Fe_6S_8(SEt)_9]$; (b) $(Et_4N)_3[Mo_2Fe_6S_9(SEt)_8]$; and (c) $(Et_3NCH_2Ph)_3[Mo_2Fe_6S_8(SEt)_3(OPh)_6]$.

also to the "linear" $[(RS)_2FeS_2FeS_2MoS_2]^{3-}$[24] cluster anions. In addition, all of these compounds have an average 2:1 ratio of second-shell Fe and Mo neighbors, respectively, per iron.

Given the above similarities for such systems, the degree of the phase cancellation of the Fe–Fe and Fe–Mo back-scattered waves, which are of approximately the same magnitude, is largely dependent upon the difference between the Fe–Fe and Fe–Mo distances, Δr, which is unique for each cluster. For example, Fourier transform of the Fe EXAFS of $(Et_4N)_3[(p\text{-}CH_3C_6H_4S)_2FeS_2FeS_2MoS_2]$[24b] ($\Delta r$ = 0.087 Å) shows a small Fe–Fe/Mo peak, whereas Fourier transforms of the Fe EXAFS of **1** (Δr = 0.036 Å),[5b] **2** (Δr = 0.028 Å),[5b] and **3** do not. Generally speaking, as we shall see later, any Mo–Fe–S cluster with a two Fe/one Mo ratio of neighbors, a small Gaussian disorder (such that $\sigma_{Fe} \approx \sigma_{Mo} < 0.1$ Å), and a distance difference of $0 \lesssim \Delta r \lesssim 0.08$ Å is not expected to show a significant Fe–Fe/Mo peak in the Fourier transform of the Fe EXAFS. In this situation, quantitative analysis of the Fe EXAFS becomes somewhat problematical, as one is now forced to deal with a mathematically ill-defined problem. We have, however, been successful in extracting structural information from the Fe EXAFS of **1**–**3** by the curve-fitting methods outlined below.

The dashed curves in Figure 3a–c show the smooth window functions applied to the Fourier transforms of **1**–**3** for Fourier filtering. The back-transformed filtered $k^3\chi(k)$ data, truncated at 3 and 14 Å^{-1} (Figures 5a–c, solid curves), were first fit (BFBT) with sulfur only (eq 1 where j = S) for **1** and **2** and with oxygen and sulfur (eq 1 where j = O, S) for **3**. The results are tabulated in Table Ib. Next, the (weak) residual Fe–Fe/Mo components were isolated via a "difference Fourier" technique.[8,24b] No Fe–Fe/Mo component could be unambiguously assigned in the Fourier transform of the difference map from the two-term fit to the filtered data of **3**. This suggests greater cancellation of Fe–Fe and Fe–Mo scattering in **3** than in **1** or **2**, which is probably due to a smaller Fe–Fe and Fe–Mo distance difference in the $MoFe_3S_4$ core of **3**.

The Fourier filtered difference spectra $k^3\chi_M(k)$, presumably containing only the Fe–Fe and Fe–Mo contributions of the total EXAFS, of **1** and **2** were curve fit with two terms (Fe and Mo) in several approximations. Nonlinear least-squares curve fitting of $k^3\chi_M(k)$ with the conventional two-term model[21c] (eq 1, j = Fe, Mo) provided accurate interatomic distances (Table Ib, worst case 1%). The accuracy of the coordination number determinations for **2**, based on **1** as the model compound, was 15% and 40% for the number of Fe and Mo neighbors, respectively, around iron. A more accurate determination of coordination numbers was not possible due both to the extremely small Fe–Fe/Mo component of the total EXAFS and to the fact that coordination number determinations are dependent on several factors (i.e., σ, $F(k)$, r) and are therefore generally less accurate than distance determinations.

The sums of the two best one-term (Fe–S) and two term (Fe–Fe and Fe–Mo) fits (dashed curves) to the total filtered EXAFS (solid curves) of **1** and **2** are shown in Figure 5a,b, respectively. Figure 5c shows the two-term (Fe–O and Fe–S) best fit (dashed curve) to the Fourier filtered data (solid curve) of **3**.

To better understand the nature of these Fe EXAFS spectra, we assume to a first approximation

$$\phi_{Mo}(k_{Mo}) = \phi_{Fe}(k_{Mo}) + \pi \qquad (2)$$

This is not an unreasonable assumption for $k \gtrsim 7$ Å^{-1}, as can be seen in Figure 4a for the total Fe–Mo phase according to Teo and Lee's calculations.[12a] Substituting for $\phi_{Mo}(k_{Mo})$ in eq 1 with this expression and simplifying with a fundamental trigonometric identity results in the very interesting numerical model

$$k^3\chi_M(k) = B_{Fe}F_{Fe}(k_{Fe})k_{Fe}^2 \exp(-2\sigma_{Fe}^2k_{Fe}^2) \sin [2k_{Fe}r_{Fe} + \phi_{Fe}(k_{Fe})]/r_{Fe}^2 - B_{Mo}F_{Mo}(k_{Mo})k_{Mo}^2 \exp(-2\sigma_{Mo}^2k_{Mo}^2) \times \sin [2k_{Mo}r_{Mo} + \phi_{Fe}(k_{Mo})]/r_{Mo}^2 \qquad (3)$$

This formulation (a *difference* of two amplitude-modulated sinusoids) clearly illustrates the cancellation of the Fe and Mo back-scatterings due to the phase difference. Curve fitting the $k^3\chi_M(k)$ data of **1** and **2**, truncated at 6 and 14.5 Å^{-1}, with this model[21c] was more susceptible to the initial set of starting vectors and to local minima than was curve fitting with the conventional model (cf. eq 1). The refined Fe–Fe and Fe–Mo distances (2.638 and 2.705 Å for **1**, respectively, and 2.705 and 2.740 Å for **2**, respectively) obtained by fitting with eq 3 are somewhat worse for **1** and essentially unchanged for **2**, when compared to the distances obtained from the fits using eq 1 (cf. Table Ib).

(24) (a) Tieckelmann, R. H.; Averill, B. A. *Inorg. Chim. Acta* **1980**, *46*, L35. (b) Teo, B.-K.; Antonio, M. R.; Tieckelmann, R. H.; Silvis H. C.; Averill, B. A. *J. Am. Chem. Soc.* **1982**, *104*, 6126.

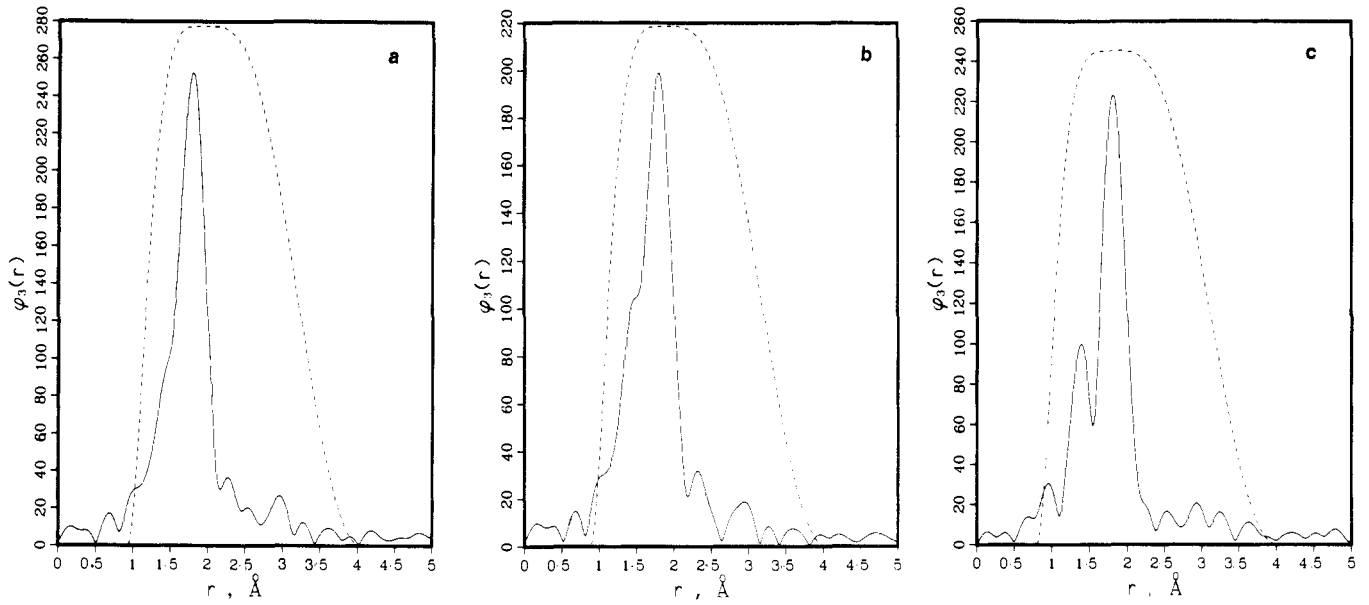

Figure 3. Fourier transforms (solid curves) $\phi_3(r)$ vs. r (Å; before phase shift correction), of the background-subtracted $k^3\chi(k)$ vs. k iron EXAFS spectra, along with the filtering windows (dashed curves), for (a) $(Bu_4N)_3[Mo_2Fe_6S_8(SEt)_9]$, (b) $(Et_4N)_3[Mo_2Fe_6S_9(SEt)_8]$, and (c) $(Et_3NCH_2Ph)_3[Mo_2Fe_6S_8(SEt)_3(OPh)_6]$.

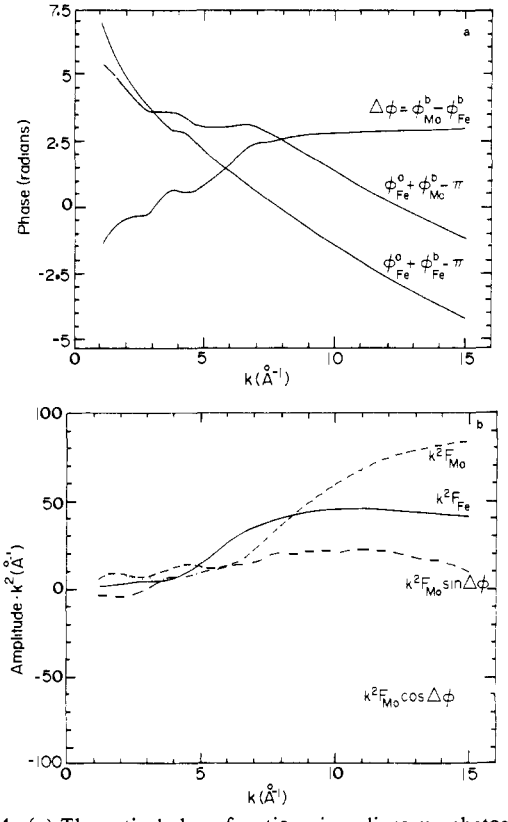

Figure 4. (a) Theoretical phase functions, in radians, vs. photoelectron wave vector k (in Å^{-1}) for the K-edge EXAFS analysis of Fe–Mo, $\phi_{Fe}{}^a + \phi_{Mo}{}^b - \pi$, and Fe–Fe, $\phi_{Fe}{}^a + \phi_{Fe}{}^b - \pi$, back-scattering components, and the total phase difference, $\phi_{Mo}{}^b - \phi_{Fe}{}^b$. (b) Theoretical amplitude functions ($F_{Mo}k^2$, and $F_{Fe}k^2$ (in Å^{-1})) vs. photoelectron wave vector k (in Å^{-1}) and the modified theoretical amplitude functions [$F_{Mo}k^2$ cos ($\Delta\phi$) and $F_{Mo}k^2$ sin ($\Delta\phi$) (in Å^{-1})] vs. k (Å^{-1}).

However, there was a considerable improvement in the number of Mo nearest neighbors to iron obtained (1.1 Mo) in the fit with eq 3. The iron coordination number (2.3 Fe) remained unchanged.

To curve fit the full data sets, 3–14.5 Å^{-1}, the approximation made in eq 2 and the model described in eq 3 could not be employed. Rather, the exact treatment gives

$$\phi_{Mo}(k_{Mo}) = \phi_{Fe}(k_{Mo}) + \Delta\phi(k_{Mo}) \quad (4)$$

in which $\Delta\phi$ is now the precise phase difference ($\phi_{Mo}{}^b - \phi_{Fe}{}^b$), as shown in Figure 4a for $1 \le k \le 15$ Å^{-1}. Substituting eq 4 into eq 1 yields

$$k^3\chi_M(k) = B_{Fe}F_{Fe}(k_{Fe})k_{Fe}{}^2 \exp(-2\sigma_{Fe}{}^2k_{Fe}{}^2) \sin [2k_{Fe}r_{Fe} + \phi_{Fe}(k_{Fe})]/r_{Fe}{}^2 + B_{Mo}F_{Mo}(k_{Mo})k_{Mo}{}^2 \exp(-2\sigma_{Mo}{}^2k_{Mo}{}^2) \times \sin[2k_{Mo}r_{Mo} + \phi_{Fe}(k_{Mo}) + \Delta\phi(k_{Mo})]/r_{Mo}{}^2 \quad (5)$$

which, after a trigonometric rearrangement, gives

$$k^3\chi_M(k) = B_{Fe}F_{Fe}(k_{Fe})k_{Fe}{}^2 \exp(-2\sigma_{Fe}{}^2k_{Fe}{}^2) \sin [2k_{Fe}r_{Fe} + \phi_{Fe}(k_{Fe})]/r_{Fe}{}^2 + B_{Mo}F_{Mo}(k_{Mo})k_{Mo}{}^2 \exp(-2\sigma_{Mo}{}^2k_{Mo}{}^2) \times \cos [\Delta\phi(k_{Mo})] \sin [2k_{Mo}r_{Mo} + \phi_{Fe}(k_{Mo})]/r_{Mo}{}^2 + B_{Mo}F_{Mo}(k_{Mo})k_{Mo}{}^2 \exp(-2\sigma_{Mo}{}^2k_{Mo}{}^2) \times \sin [\Delta\phi(k_{Mo})] \cos [2k_{Mo}r_{Mo} + \phi_{Fe}(k_{Mo})]/r_{Mo}{}^2 \quad (6)$$

Two new trigonometric terms containing the phase difference, cos [$\Delta\phi(k_{Mo})$] and sin [$\Delta\phi(k_{Mo})$], appear in eq 6, and it is obvious that, for $\Delta\phi = \pi$, eq 6 reduces to eq 3. These modified amplitude functions $F_{Mo}(k)k_{Mo}{}^2$ cos [$\Delta\phi(k)$] and $F_{Mo}(k)k_{Mo}{}^2$ sin [$\Delta\phi(k)$] are plotted in Figure 4b. The product of the cosine term is *negative* for $6 \lesssim k \lesssim 15$ Å^{-1}, and the product of the sine term is slightly *positive* for $3 \lesssim k \lesssim 15$ Å^{-1}. Note that the former term outweighs the latter term.

This model is useful primarily in that it presents the most accurate description of the problem, i.e., phase and amplitude cancellation of Fe–Fe/Mo backscattering in Mo–Fe–S clusters. Curve fitting with eq 6 yields results similar to those obtained from the conventional two-term model eq 1, cf. Table Ib. This is to be expected because, after all, there is essentially no difference between the two approaches, eq 1 and 5 (or 6). That is, the phase function $\phi_{Mo}(k_{Mo})$ in eq 1 is replaced by an alternate but exact expression (eq 4) in eq 5. The stepwise approach, however, helps to alleviate false minima and/or ill-behaved problems.

The sum of the iron and molybdenum back-scattering terms can also be combined into a single term (according to an extension of the EXAFS beat node method developed by Martens et al.[25]) of the form

(25) Martens, G.; Rabe, P.; Schwentner, N.; Werner, A. *Phys. Rev. Lett.* **1977**, *39*, 1411.

(26) (a) Antonio, M. R.; Teo, B.-K.; Averill, B. A., manuscript in preparation. (b) Cleland, W. E.; Averill, B. A. *Inorg. Chem. Acta* **1981**, *56*, L9. (c) Cleland, W. E.; Sabat, M.; Ibers, J. A.; Averill, B. A., submitted for publication.

$$k^3\chi_M(k) = k^2\tilde{A}_M(k) \sin [2k\bar{r} + \tilde{\phi}_M(k)] \quad (7)$$

Here $\bar{r}$ is the average interatomic distance as given by $\bar{r} = (r_{Fe-Fe} + r_{Fe-Mo})/2$, and $\tilde{A}_M(k)$ is a modified back-scattering amplitude function that can be written as

$$\tilde{A}_M(k) = A_{Fe}(k)[1 + C^2(k) + 2C(k) \cos[2k\Delta r + \Delta\phi(k)]]^{1/2} \quad (8)$$

$\tilde{\phi}_M(k)$ is the correspondingly modified phase function

$$\tilde{\phi}_M(k) = \phi_{Fe}(k) + \arctan\left[\frac{C(k) \sin[k\Delta r + \Delta\phi(k)] - \sin(k\Delta r)}{C(k) \cos[k\Delta r + \Delta\phi(k)] + \cos(k\Delta r)}\right] \quad (9)$$

$A_{Fe}(k)$ and $\phi_{Fe}(k)$ are the unmodified amplitude envelope

$$A_{Fe}(k) = \frac{N_{Fe}F_{Fe}(k)}{r_{Fe-Fe}^2} \exp(-2\sigma_{Fe}^2k^2) \quad (10)$$

and phase function, respectively, for iron. The function $C(k)$ is the ratio of the molybdenum and iron amplitude envelopes:

$$C(k) = \frac{N_{Mo}}{N_{Fe}} \frac{F_{Mo}(k)}{F_{Fe}(k)}\left[\frac{r_{Fe-Fe}}{r_{Fe-Mo}}\right]^2 \exp[-2(\sigma_{Mo}^2 - \sigma_{Fe}^2)k^2] \quad (11)$$

The distance and phase differences (Δr and $\Delta\phi(k)$, respectively) are given by $\Delta r = r_{Fe-Mo} - r_{Fe-Fe}$ and $\Delta\phi(k) = \phi_{Mo}^b(k) - \phi_{Fe}^b(k)$. The modified EXAFS functions presented in eq 8 and 9 are of most concern to us here as guides for predicting how the degree of amplitude and phase cancellation of Fe–Fe and Fe–Mo back-scattered waves depends on the Fe–Fe and Fe–Mo distances in **1**–**3** and other related systems.

For the ratio $N_{Mo}/N_{Fe} = {}^1/_2$, the square root term of $\tilde{A}_M(k)$ in eq 8 and the arc tangent term of $\tilde{\phi}_M(k)$ in eq 9 have been calculated; the results for $\tilde{A}_M(k)/A_{Fe}(k)$ and $\tilde{\phi}_M(k) - \phi_{Fe}(k)$ are shown in Figure 6, a and b, respectively, for six values of Δr = 0.0, 0.02, 0.04, 0.06, 0.08, and 0.1 Å. Other relevant input parameters are (i) the Debye–Waller factors, σ_{Mo} = 0.069 Å and σ_{Fe} = 0.076 Å, (ii) the Fe–Fe distance was fixed at r_{Fe-Fe} = 2.693 Å, from which the Fe–Mo distances were obtained in 0.02-Å increments, such that $r_{Fe-Mo} \geq r_{Fe-Fe}$ and (iii) the theoretical amplitude and phase functions of Teo and Lee.[12a]

The modified amplitude functions, $\tilde{A}_M(k)/A_{Fe}(k)$ in Figure 6a, exhibit shallow minima that are presumably associated with the beating in the EXAFS amplitude due to the superimposed Fe–Fe and Fe–Mo back-scattered waves of different frequencies. The positions of the beat frequencies shift to lower k (Å^{-1}) with increasing distance differences (Å). The corresponding modified phase functions $\tilde{\phi}_M(k)$ - $\phi_{Fe}(k)$ are shown in Figure 6b. The modified amplitude $\tilde{A}_M(k)$ is considerably smaller than $A_{Fe}(k)$ as shown by the ratio $\tilde{A}_M(k)/A_{Fe}(k)$, which is less than 1 over a large range of k for values of Δr = 0 to ca. 0.06 Å (cf. Figure 6a). Note that for N_{Mo}/N_{Fe} = 0.5, one expects $\tilde{A}_M(k)/A_{Fe}(k)$ = 1.5 if everything else is equal for the two terms (i.e., $C(k) = N_{Mo}/N_{Fe}$ = 0.5; cf. eq 11). It is apparent from eq 8 that amplitude cancellation ($\tilde{A}_M(k)/A_{Fe}(k) < 1.5$) can occur if the combination of distance and phase differences is such that cos $(2k\Delta r + \Delta\phi(k))$ is negative. Conversely, amplitude enhancement ($\tilde{A}_M(k)/A(k) > 1.5$) can occur if $F_{Mo}(k) > F_{Fe}(k)$ and/or $\sigma_{Mo} < \sigma_{Fe}$ and/or $r_{Fe-Fe} > r_{Fe-Mo}$. For example, at Δr = 0 and 0.02 Å, $\tilde{A}_M(k)/A_{Fe}(k)$ is less than 1 for $6 \lesssim k \lesssim 15$ Å^{-1}. When the distance difference exceeds approximately 0.08 Å, the ratio rises steeply above 1 at ca. 10 Å^{-1}. Using Figure 6a,b and the known Δr values of 0.036, 0.028, and 0.087 Å for complexes **1**,[5b] **2**,[5b] and $[S_2MoS_2FeS_2Fe(S\text{-}p\text{-}CH_3C_6H_4)_2]^{3-}$,[24b] it is understandable that only the last compound, which has the largest Δr, exhibits a small Fe–Fe/Mo peak in the Fourier transform of the Fe EXAFS. One can also predict that an Fe–Fe/Mo peak will be expected to be weak or unobservable for $0 \lesssim \Delta r \lesssim 0.08$ Å with the combination of bond ratio and distances typical of the Mo–Fe–S clusters under consideration.

The regression coefficients for the ΔE_0 vs. Δr and the B vs. σ correlation curves of Fe–O and Fe–S interactions are tabulated in Table IIc (cf. supplementary material) and the FABM results are listed in Table IIIc (cf. supplementary material). The corresponding data for the Fe–Fe and Fe–Mo interactions cannot be obtained owing to their vanishingly small EXAFS contribution (and hence ill-behaved correlation curves).

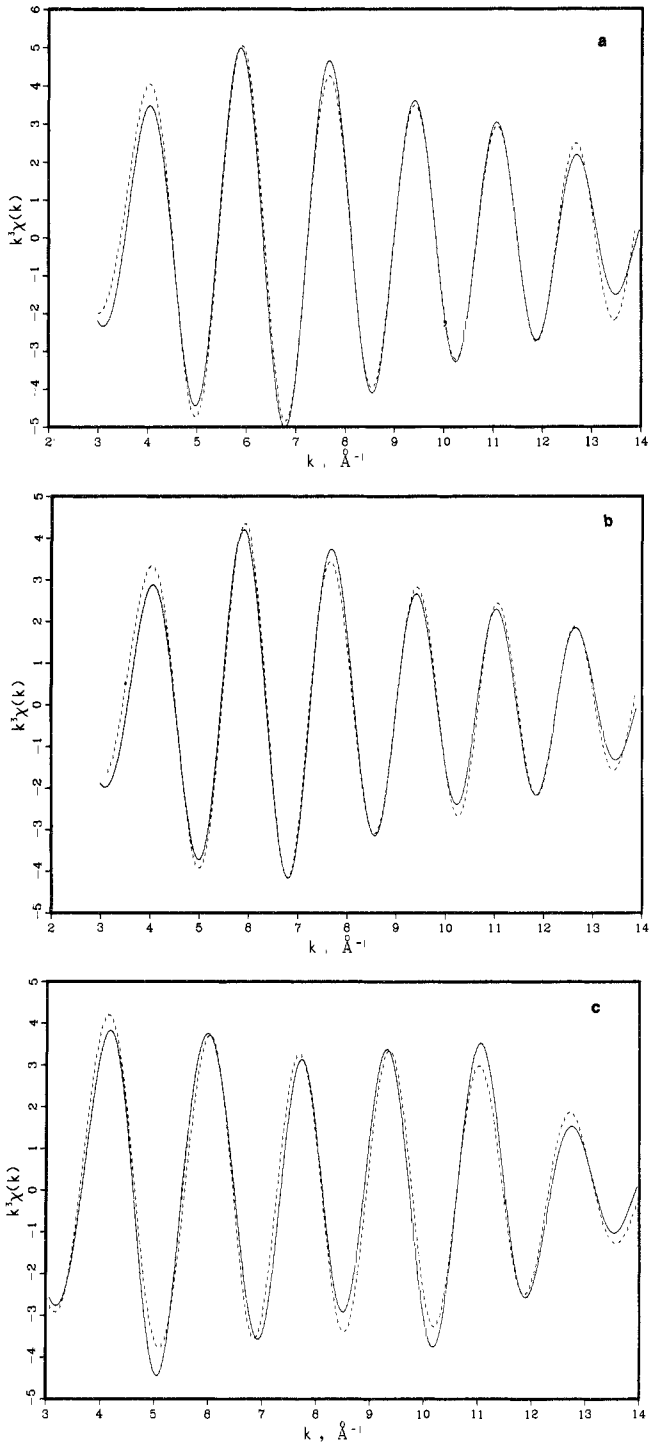

Figure 5. Fourier filtered $k^3\chi(k)$ vs. k iron EXAFS spectra (solid curves) and the nonlinear least-squares best fits (dashed curves), based on theoretical functions, of (a) the sum of both the one-term (Fe–S) and two-term (Fe–Fe, Fe–Mo) curve fittings to the data of $(Bu_4N)_3[Mo_2Fe_6S_8(SEt)_9]$; (b) the sum of both the Fe–S and the Fe–Fe and Fe–Mo curve fittings, as above, to the data of $(Et_4N)_3[Mo_2Fe_6S_9(SEt)_8]$; and (c) the two-term (Fe–O, Fe–S) fit to the data of $(Et_3NCH_2Ph)_3[Mo_2Fe_6S_8(SEt)_3(OPh)_6]$.

Conclusions

The Mo and Fe K-edge EXAFS of three Mo–Fe–S double-cubane type clusters have been measured and interpreted. The molybdenum EXAFS clearly establishes the presence of a sym-

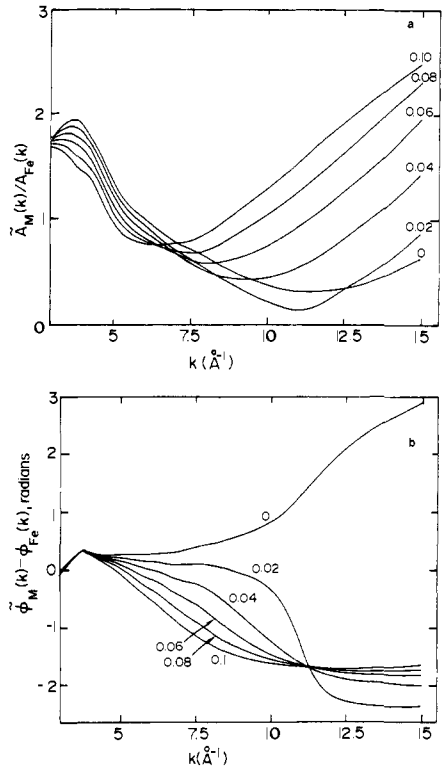

Figure 6. (a) Modification of amplitude envelope function $\tilde{A}_M(k)/A_{Fe}(k)$ vs. photoelectron wave vector (in Å^{-1}) for six distance differences, Δr = 0, 0.02, 0.04, 0.06, 0.08, and 0.1 Å. (b) Modification of phase function, $\tilde{\phi}_M(k) - \phi_{Fe}(k)$, vs. photoelectron wavevector, k (in Å^{-1}) for six distance differences, as in a.

metrical Mo(μ_2-SEt)$_3$Mo bridging unit in the new cluster **3**, the phenolate analogue of **1**. Curve fitting the Mo EXAFS with two- and three-term expressions yields average sulfide distances and coordination numbers with the former treatment and both average sulfide and thiolate distances and coordination numbers in the latter treatment, in addition to the corresponding Mo–Fe details. Our present results for the Mo EXAFS of $[Mo_2Fe_6S_8(SEt)_9]^{3-}$ (**1**) and $[Mo_2Fe_6S_9(SEt)_8]^{3-}$ (**2**) show that the original Mo EXAFS of **2** reported in the literature was in fact that of an approximately equimolar mixture of **1** and **2**.

The anomalous feature observed in the Fourier transforms of the Fe EXAFS of these systems, namely the lack of an Fe–Fe/Mo peak, has been explained principally in terms of the phase cancellation of two nearly equivalent back-scattering waves. In a novel extension of the EXAFS beat method, modified amplitude envelope and phase functions were calculated to illustrate dependence of the cancellation of the Fe–Fe and Fe–Mo corresponding back-scattered waves upon the Fe–Fe and Fe–Mo distances. The Fe EXAFS was curve fit with both conventional and novel descriptions of this ill-defined phase (and amplitude) problem. In each case, acceptable interatomic distances were obtained from the refinements, but because so much of the Fe–Fe/Mo component to the total EXAFS is lost, accurate coordination number determinations were not always possible.

It should be emphasized that the Mo–S/S′ interactions of the Mo EXAFS as well as the Fe–Fe/Mo interactions of the Fe EXAFS of these double-cubane clusters (**1–3**) are ill-defined problems in EXAFS due to the interference of two waves similar in amplitude and phase (as in the case of Mo–S and Mo–S′ of Mo edge) or of two waves similar in amplitude but approximately out of phase by π radians (as in the case of Fe–Fe and Fe–Mo of Fe edge). Such interference can lead to one or more of the following characteristics: (1) multiple minima (as in the Mo edge of **2**); (2) unusual characteristic numbers (ΔE_0*, σ*, S*), notably the unusually small amplitude reduction factors (e.g., S* of ca. 0.32 for Mo–S of **1–3** is significantly smaller than that of 0.59[12e] for Mo–S of a number of Mo–Fe–S clusters containing the MoS_4 unit); (3) ill-behaved correlation functions, especially the B vs. σ curves (as in the case of **2** and the Fe–Fe/Mo of **1–3**); and in extreme cases (4) total or nearly total disappearance of the EXAFS signal (as in the case of the Fe–Fe/Mo interactions in the Fe edge of **1–3**). As demonstrated in this paper, though reasonable distance information can still be obtained for these ill-behaved systems either by multiple-term fitting or by a "difference Fourier" technique, the accuracy for the coordination numbers is poor. Furthermore, while reasonably accurate structural parameters can be determined by EXAFS within this set of closely related clusters, transferability of the phase and amplitude information to and from other systems for these ill-behaved systems should be treated with extreme caution.

Finally it is evident from the Fourier transforms of the Fe EXAFS of **1–3** that these clusters (which contain the $MoFe_3S_4$ core structure) are inadequate as models for the more complex Fe–Fe/Mo feature present in the FeMo cofactor spectrum.

Acknowledgment. This research was supported in part by a grant to B.A.A. from the USDA/SEA Competitive Research Grants Office (5901-0410-8-0175-0). We thank the staff at CHESS for their assistance. SSRL is supported by the NSF through the Division of Materials Research and the NIH through the Biotechnology Resource Program in the Division of Research Resources in cooperation with the Department of Energy.

Registry No. **1**, 85369-95-5; **2**, 67583-54-4; **3**, 85369-97-7.

Supplementary Material Available: Tables of the raw X-ray absorption data in the form μX vs. E (in eV), Figures A–G, the background-subtracted Mo and Fe EXAFS spectra $k^3\chi(k)$ vs. k (in Å^{-1}) for **1–3**, Table II, regression coefficients of the correlation curves, and Table III, FABM results of distances and coordination numbers (38 pages). Ordering information is given on any current masthead page.